ハイパースペクトルデータを用いた術中脳表酸素飽和度可視化手法 ： 2次元マッピング法

森，恩

Intraoperative Visualization of Cerebral Oxygenation Using Hyperspectral Image Data: A Two-Dimensional Mapping Method

Megumu Mori[1], Toru Chiba[2], Akira Nakamizo[1], Ryuichi Kumashiro[3], Masaharu Murata[4], Tomohiko Akahoshi[5], Morimasa Tomikawa[3], Yuichirou Kikkawa[1], Koji Yoshimoto[1], Masahiro Mizoguchi[1], Tomio Sasaki[1], Makoto Hashizume[5]

[1]Department of Neurosurgery, Graduate School of Medical Sciences, Kyushu University, Fukuoka, Japan

[2]HOYA Corporation, PENTAX Life Care Division, Tokyo, Japan

[3]Department of Advanced Medicine and Innovative Technology, Kyushu University Hospital, Fukuoka, Japan

[4]Innovation center for Medical Redox Navigation, Kyushu University, Fukuoka, Japan

[5]Department of Advanced Medical Initiatives, Graduate School of Medical Sciences, Kyushu University, Fukuoka, Japan

Corresponding author: Makoto Hashizume, M.D., Ph.D., F.A.C.S.

3-1-1 Maidashi, Higashi-ku, Fukuoka 812-8582, Japan

Tel: +81-92-642-5992

Fax: +81-92-642-5199;

Email: mhashi@dem.med.kyushu-u.ac.jp

Abstract

Purpose.

Superficial temporal artery (STA)-middle cerebral artery (MCA) bypass is an important technique for cerebrovascular reconstruction. Intraoperative hemodynamic imaging is needed to perform cerebrovascular reconstruction safely and effectively. Optical intrinsic signal (OIS) imaging is commonly used for assessing cerebral hemodynamics in experimental studies, because it can provide high resolution mapping images. However, OIS is not used clinically due to algorithm, instrumentation and spectral resolution limitations. We tested the feasibility of a hyperspectral camera (HSC) for assessment of cortical hemodynamics with spectral imaging of the cerebral cortex in rats and in vivo humans.

Methods.

A hyperspectral camera (HSC) was tested in a rat model of cerebral ischemia (middle cerebral artery occlusion) and during human revascularization surgery (STA-MCA anastomosis). Changes in cortical oxygen saturation were derived from spectral imaging data (400-800 nm) collected by exposing the cortex to Xenon light. Reflected light was sampled using the HSC. The system was then tested intraoperatively during superficial temporal artery to middle cerebral artery anastomosis procedures. Comparison with single photon emission computed tomography (SPECT) imaging data was done.

Results.

During middle cerebral artery occlusion in rats, the HSC technique showed a significant decrease in cortical oxygen saturation in the ischemic hemisphere. In clinical cases, the cortical oxygen saturation was increased after STA-MCA anastomosis, which agreed with the SPECT imaging data.

Conclusion.

Continuous collection of imaging spectroscopic data is feasible and may provide reliable quantification of the hemodynamic responses in the brain. The HSC system may be useful for monitoring intraoperative changes in cortical surface hemodynamics during revascularization procedures in humans.

Key words: optical intrinsic signal image; visible light spectroscopy; oxygen saturation; misery perfusion; hyperspectral camera; continuous spectral data,

Introduction

Extracranial-intracranial (EC-IC) bypass, such as superficial temporal artery (STA)-middle cerebral artery (MCA) bypass, has been recognized as an important technique for cerebrovascular reconstruction, and the procedure has become a standard surgical therapeutic option for patients suffering from moyamoya disease with transient ischemic attack (TIA) to prevent stroke [1-3]. To ensure that cerebrovascular reconstruction can be performed safely and effectively, the cerebral ischemia induced by the temporary recipient artery and hyperperfusion state induced by the STA-MCA bypass should be considered. The intraoperative cerebral blood flow changes during STA-MCA bypass could be confirmed by a near-infrared analysis using indocyanine green (ICG) [4] or laser speckle imaging [5-7], but these methods could not evaluate the cerebral cortical metabolic changes. Postoperative radioisotope examinations with positron emission tomography (PET) are most commonly used to assess the metabolic changes in the brain, but this type of examination cannot be performed during surgery. Thus, there is a need for novel intraoperative imaging tools to detect the cortical neuronal metabolism during cerebrovascular reconstruction, and spectral analysis techniques have been studied as one such technique [8,9].

The hyperspectral imaging remote sensing technology was initially developed by the U.S. National Aeronautics and Space Administration (NASA) for monitoring the earth's resources. Hyperspectral image data are often compared with data from a spectral image cube, in which positional information exists in the xy plane, and wavelength information exists in the z direction [10-12]. The spectral image cube data can be recognized as an image at each wavelength, and with spectra at every pixel. This technology has been employed in various fields of research [13], and has more recently

been used in the neurological research field, such as using the Optical Intrinsic Signal (OIS) imaging technique. According to previous research, the intraoperative OIS imaging technique has the capacity to assess the cerebral hemodynamics during neurological surgery for cerebrovascular lesions (e.g., arteriovenous malformation, cavernous malformation, intracranial ischemic lesions, etc.) [8,9]. Having such hemodynamic information during surgery would help to improve the safety of the operation.

Although OIS imaging can provide high resolution mapping images, the accuracy has not yet reached a level high enough for clinical application. This inaccuracy is thought to be based on the limitations associated with the algorithms, instrumentation and spectral resolution. For example, OIS requires the use of band-pass filters to extract specific wavebands of interest of the cortical surface, which results in other wavelengths being ignored (e.g., other chromophores, scattering and so on) [14-17]. To overcome this obstacle associated with the past OIS techniques, some papers have studied the spectral analysis [18,19]. We used a hyperspectral camera (HSC) to capture the continuous spectral data (hyperspectral image data) of the cortical surface over the visible light band (400-800 nm) and adopted the modified Lambert–Beer algorithm to convert the changes of the OIS to changes in the concentrations of oxy-hemoglobin and deoxy-hemoglobin while analyzing the collected spectral data.

The aim of this study was to determine whether we could perform spectral mapping imaging of the cerebral cortical surface hemodynamics using two-dimensional spectral data (termed 'hyperspectral data'), and whether such data would be suitable for clinical use. We first performed *in vitro* studies to confirm the correlation between the

hyperspectral data for hemoglobin (Hb) and the other popular spectroscopic techniques.

Next, we evaluated the rat brain hemodynamics during normal perfusion and cerebral

ischemia to assess the validity of the hyperspectral measurement of the cortical surface

Hb (captured using a HSC). Finally, we confirmed that this technique was practical for

measuring the cortical surface hemodynamic changes during revascularization

procedures in human patients.

Methods

HSC capture system

A F1.4 50 mm lens was attached to the HSC (HSC1700; Eba Japan, Tokyo, Japan)

using a mount adapter, and the capture procedure was controlled by a connected

computer. Xenon (XEF-152S Kenko, Tokyo, Japan) was employed as a light source.

All the spectra were calibrated using reference data, which were collected as the

reflected light of a $BaSO_4$ standard (white) (Eq. 1):

$$O(\lambda_i) = \frac{R(\lambda_i)}{W(\lambda_i)}$$

$(i = 0,1,2\cdots,80)$

$$\lambda_0 = 400nm, \lambda_1 = 405nm, \lambda_2 = 410nm...\lambda_{80} = 800nm$$

O: observed spectrum
R: collected spectrum data of HSC
W: reference spectrum   (Eq. 1)

The HSC1700 (Fig. 1) was developed as a spin-off product of an Earth observation microsatellite technology demonstration mission under development at the Hokkaido Institute of Technology, Sapporo, Hokkaido, Japan (https://directory.eoportal.org/web/eoportal/satellite-missions/t/taiki)[20]. It takes about five to 16 seconds to capture the entire spectral imaging cube, depending on the capture size. In case coarse displacement errors occurred when capturing the spectral imaging cube data, we re-collected the data to ensure that it was acceptable for the analysis.

Normalization of spectral data

Before the data were processed, a three-point moving average was applied to each spectrum for smoothing. Thus, all reflectance spectral data points were reconstructed in 5-nm steps, and we selected the data for the wavelengths from 405 to 750 nm for the analysis. As the surface of human tissues exhibits unexpected undulations, the measured spectral data are affected by the distance and angle of each point. Thus, normalization procedures are required for the recognition of spectral data (Eq. 2):

$$O'_{(\lambda_i)} = \left(\frac{O_{(\lambda_0)}}{\sum_i O_{(\lambda_i)}}, \frac{O_{(\lambda_1)}}{\sum_i O_{(\lambda_i)}}, \cdots \frac{O_{(\lambda_{80})}}{\sum_i O_{(\lambda_i)}} \right)$$

O' : normalized spectrum
O : observed spectrum
$\sum_i O_{(\lambda_i)}$: total spectrum intensity (Eq. 2)

The equation "$\Sigma O(\lambda i)$" represents the integration of the spectral intensity of the observed wavelength area (405-795 nm). Consequently, "$\Sigma O(\lambda i)$" is proportional to the reflection intensity, which is attenuated by the surface conditions. To ensure the

concentration linearity of the components, the data were transformed from reflection (%) to absorption (-log (I/I0)) according to the modified Beer-Lambert's law. The calculations of the hemoglobin saturation and scatter effect have already been demonstrated in several previous studies [21-25].

Oxygen saturation data processing

Typical oxy-hemoglobin (HbO) and deoxy-Hb (HbR) features are observed between 522 to 588 nm. The processing procedures used for this spectral feature were reported previously [26]. The multiple regression analysis methods comprise a group of statistical, mathematical or graphical techniques that analyze multiple variables simultaneously [27].

For the spectra of the human cerebral surface, spectral components are mathematically controlled by the main powers of HbO, HbR, scatter and offset. The spectral data for these four components were prepared separately. For the scattering model, we employed a mathematical equation as follows (Eq. 3):

$$scatter(\lambda_j) = A\left(\frac{\lambda_j}{\lambda_{69}}\right)^{-B} + C\left(\frac{\lambda_j}{\lambda_{69}}\right)^{-4}$$

$$j = 0, 1 \cdots 69$$
$$(\lambda_0 = 405, \lambda_2 = 410 \cdots \lambda_{69} = 750 nm)$$

(Eq. 3)

The first term on the right-hand side of this expression is related to the Mie scatter, which is commonly used as scatter model for cells and tissues. The second term is related to the scattering from Rayleigh particles. The reflectance spectra were analyzed

using the diffusion approximation model [26]. The unmatched component in the

spectrum is treated as a residual in this method (Eq. 4):

$$
\begin{pmatrix} X_{(\lambda_0)} \\ X_{(\lambda_1)} \\ \vdots \\ X_{(\lambda_{69})} \end{pmatrix} = coeff_{HbR} \times \begin{pmatrix} HbR'_{(\lambda_0)} \\ HbR'_{(\lambda_1)} \\ \vdots \\ HbR'_{(\lambda_{69})} \end{pmatrix} + coeff_{HbO} \times \begin{pmatrix} HbO'_{(\lambda_0)} \\ HbO'_{(\lambda_1)} \\ \vdots \\ HbO'_{(\lambda_{69})} \end{pmatrix} + \begin{pmatrix} scatter_{(\lambda_0)} \\ scatter_{(\lambda_1)} \\ \vdots \\ scatter_{(\lambda_{69})} \end{pmatrix} + offset + residual
$$

$$j = 0,1 \cdots 69$$

$$(\lambda_0 = 405, \lambda_2 = 410 \cdots \lambda_{69} = 750 nm)$$

(Eq.4)

Consequently, a coefficient for each component is obtained, and those of HbR and HbO

are shown in the Figures as $coeff_{HbR}$ and $coeff_{HbO}$. The value of each coefficient

corresponds to their component data. Value of B and C in scatter equation (Eq. 3) are

optimized by nonlinear least-squares algorithm, we employed conjugated gradient

method. The software program was prepared utilizing MATLAB/OCTAVE code. After

B.C value was fixed, coefficients of HbR and HbO were calculated by least square

method. These procedures were shown in Figure 2. Basically, the observed spectral data

should be the sum of the multiplication of each component and co-efficient in this

method. Therefore, from the value of the coefficients of HbR and HbO, it is possible to

estimate the relative hemoglobin concentration (rHb-c) and oxygen saturation as

follows (Eq. 5, 6):

$$relative\_Hb\_concentration = coeff_{HbR} + coeff_{HbO} \qquad\qquad \text{(Eq. 5)}$$

$$oxygen\_saturation = \frac{coeff_{HbO}}{coeff_{HbR} + coeff_{HbO}}$$

<div align="right">(Eq. 6)</div>

In the calculation of the relative hemoglobin concentration and saturation of hemoglobin (Eq. 5, 6), a coefficient of scatter and offset was not used, but in the calculation process, the accuracy of the coefficient values are obviously affected by the component choice. The required component data should therefore not be reduced, even if they are not needed later. The appropriate coefficients for these linear combinations were then linearly correlated with the oxygen saturation (measured by a spectrometer) and the saturation value (calculated from HSC data) of the hemoglobin samples (diluted with normal saline and oxygenated blood). A comparison of the results obtained with the HSC and their respective calibrations is shown in Figure 3. The correlation coefficient was $R^2=0.998$ for oxygen, thus corresponding to a standard error of prediction of 7.31%.

Oxygen saturation mapping images

A saturation value of 640×480 data points (pixels) was calculated for less than 10 seconds, and a two-dimensional oxygen saturation figure was produced.

The volume of rHb-c was expressed by consecutive colors in the Hb maps, where red indicated a high volume of rHb-c, yellow indicated a moderate volume of rHb-c and blue indicated a low volume of rHb-c. The value of oxygen saturation was also expressed by consecutive colors in the oxygen saturation maps. Deep red meant that the value of oxygen saturation was nearly100%, yellow meant that it was nearly 50% and deep blue meant that it was nearly 0%.

Animal studies

Animal preparation

Male Wistar rats (n=7) weighing 300-450 g were studied in accordance with the Institution Animal Care and Use Committee of the Kyushu University Graduate School of Medical Sciences. Animals were anesthetized with 2.5-3.0% isoflurane, and anesthesia was maintained with 2.0% isoflurane in 75% N_2O and 25% O_2 using a face-mask. The room air conditioner was set as 25°C, and the body temperature was maintained at 37±0.5°C throughout the procedure using a heating mat.

Under a stereomicroscope, a surgical skin incision was made on the rat's head, and a 5×5 mm bone window was made in the exposed region (2.5 mm bilateral and 1 mm anterior to the bregma, and 1 mm posterior to the lambda) with an electrical drill. To observe the cortical surfaces, we exposed the brain surface to a xenon light and observed the reflection using the HSC. We set three regions of interest (ROIs) on each cortical parenchymal area in the saturation map, which were downstream of the MCA. We avoided setting ROIs on structures such as blood vessels. The anatomical structures were used so that almost the same place (ROI) could be pinpointed in each animal. The size of the ROIs consisted of 20 x 20 pixels. We extracted oxygen saturation data for 20 × 20 pixels from each side of the cortical surfaces in both hemispheres that were in the MCA territory, and the mean values of ROIs were calculated. The average value of each ROI was treated as the value representative of the ROIs.

Ischemic model

We utilized the middle cerebral artery occlusion (MCAO) technique [28] to develop our cerebral ischemia model. In this study, we performed right hemisphere MCAO. A silicon-coated nylon suture (SSK-R1 Doccol Co., Sharon, MA, USA) was used to perform the right MCAO. The brains were removed 12 h after the MCAO technique, and the infarction was identified with 2,3,4-triphenyltetrazolium chloride (TTC) [29]. Using a rat brain slicer (Rodent brain matrix, Adult Rat, Coronal Sections; ASI Instruments, Warren, MI, USA), 3 mm coronal sections were dissected at a distance of 2, 5, 8 and 11 mm from the frontal pole. After sectioning, the slices were immediately immersed in 2% TTC in 0.9% NaCl at 37°C for 10 min.

In vivo data collection and analysis

The collection of the spectral image data of the cerebral surface was performed with the HSC capture system just after the craniotomy and again 20 min after the right MCAO (the cerebral blood flow was previously reported to be stable 20 min after MCAO [27]). The statistical significance of differences in the mean HSC data (oxygen saturation data) between the pre- and post-MCAO periods were evaluated by a two-sided t-test with Welch's correction. The blood flow velocities (BFV) of each middle cerebral artery were measured at the half point of the MCA by ultrasonography (EUB-5500, HITACHI-Medico, Tokyo, Japan). The flow velocity measurement was performed almost simultaneously with the HSC capture. The statistical significance of differences in the BFV between the pre- and post-MCAO data were evaluated by the two-sided t-test. The statistical analysis was performed using the GraphPad Prism v.6 software program for Mac (GraphPad, San Diego, CA, USA).

Clinical study

This study was approved by the Kyushu University Ethical Review Board, and included

the collection of scan data from clinical cases. Informed consent was obtained from all

patients prior to both surgery and intraoperative intrinsic optical imaging.

Patient characteristics

We investigated four patients undergoing STA-MCA anastomoses during the period

from November 2011 to December 2012 at Kyushu University Hospital. The subjects

included two patients with moyamoya disease and two with occlusion of the ICA. All

individual patient profiles are shown in Table 1.

Single photon emission computed tomography (SPECT) was performed for three

of the patients, excluding an IC occlusion patient in the subacute phase of cerebral

infarction. SPECT revealed a reduced regional CBF (rCBF) at rest ($\leq$ 30 ml per 100

g/min) and vasoreactivity to acetazolamide ($\leq$10%) in all three patients.

HSC in clinical cases

To observe the cortical surfaces, we exposed the brain surface to a xenon light and

observed the reflection using the HSC. The HSC captures were performed twice per

case. The first scan was performed when the cerebral surface was exposed, and the

second was performed just after the STA-MCA anastomosis. We set six regions of

interest (ROIs) on the cortical surface, which were in the territory downstream of the

STA-MCA anastomosis, in consideration of the relevance of the ischemic region after

surgery. We avoided structures such as blood vessels when setting the ROIs. The

anatomical structures were used so that the almost same location (ROIs) could be

pinpointed for the different scans. We extracted ROI data from regions of 20×20 pixels in the oxygen saturation maps, and the mean HSC data were calculated. The average value of each ROI was treated as the value representative of the ROIs. The statistical significance of differences in the mean HSC data (oxygen saturation) between the pre- and post-STA-MCA anastomosis periods were evaluated by a two-sided t-test with Welch's correction.

Results

Animal study

The evaluation of the blood flow changes during the MCAO procedure by ultrasound showed an obvious decrease in the BFV of the rt. MCA after MCAO (Fig. 4). The peak flow velocity, mean flow velocity and diastolic flow velocity decreased 20 minutes after MCAO, and these results were similar to those in a previous study [30]. A brain infarction was confirmed by TTC staining 12 h after MCAO (Fig. 5). TTC reflects the metabolism of the mitochondria, so ischemic regions are not dyed. Therefore, the TTC staining showed that the area downstream of the MCA was obviously infarcted.

The spectral data obtained with the HSC capture system could be converted to both Hb and oxygen saturation mapping figures (Fig. 6). The yellow-colored area decreased in the right hemisphere, which was the MCAO side, in the Hb maps, confirming that the volume of rHb-c was reduced after the MCAO procedure (Figs. 6B, 6E). The blue-colored area for the saturation increased on the same side, thus showing that the saturation was also reduced after the MCAO procedure in the oxygen saturation maps (Figs. 6C, 6F). The locations of the ROIs are shown in figure 7. The saturation values of the ischemic hemisphere were clearly decreased compared with those of the

control hemisphere (Fig. 8). The oxygen saturation of the right post-procedure

hemisphere was significantly lower than that of the left post-procedure hemisphere (p<

0.01). The oxygen saturation of the right post-procedure hemisphere was also

significantly lower than that of the right pre-procedure hemisphere (p< 0.01).

Clinical study

In the clinical cases, the HSC data could also be converted to Hb-related images (rHb-c

mapping images and oxygen saturation images) (Fig. 9). Furthermore, we were able to

display these images within several seconds to the surgeons during the operation.

Although it was slightly demanding to intuitively understand a change of the blood

volume based on the rHb-c mapping image (Figs. 9B, 9E), the visual evaluation of the

changes in oxygen saturation (oxygen-saturation mapping image) was simple (Figs. 9C,

9F). The red-colored area increased in the rHb-c map, therefore, the volume of rHb-c

was increased after the STA-MCA anastomosis (Figs. 9B, 9E). The red-colored area

also increased in the same area for the oxygen saturation map, thus confirming that the

value of the saturation also increased after the STA-MCA anastomosis (Figs. 9C, 9F).

The locations of the ROIs are shown in figure 10.

As expected, the oxygen saturation determined from the mean HSC data increased

after the STA-MCA anastomosis (Fig. 11). The oxygen saturation of the postoperative

cortex was significantly higher than that of the preoperative cortex (p<0.001). At around

two weeks after the operation, SPECT was also performed in three patients.

Unfortunately, one case with bilateral IC occlusion died one day after the operation

because of acute renal failure, and thus could not be analyzed. SPECT in the remaining

three cases revealed an improved regional CBF (rCBF) at rest (> 30 ml per 100 g/min) and vasoreactivity to acetazolamide (>10%).

Discussion

Cerebral cortical hemodynamic evaluation

During cerebrovascular reconstruction surgery in patients with hemodynamic ischemia, the cerebral blood volume (CBV) has been reported to increase in order to compensate for the decreased cerebral blood flow (CBF), and that the oxygen extraction fraction (OEF) increases to maintain the neuronal metabolism [31], in a phenomenon termed "misery perfusion" [32]. In our clinical study using the HSC, we confirmed that the oxygen saturation of the cortical surface was decreased before the revascularization procedure, and that it increased after the revascularization procedure, thus suggesting that the cerebral blood flow and the OEF had improved and normalized, and that the oxygen saturation had also increased. Although there have been a number of studies using near-infrared spectroscopy to assess the cortical hemodynamics during EC-IC bypass surgery [33-35], there have been limited reports on the use of visible light spectroscopy, and those have only used a probe-type wavelength collection system [35]. As a result, to our knowledge, this is the first report of the use of visible light spectroscopy to determine the saturation changes of the cortical surface by oxygen-saturation mapping imaging of the misery perfusion state. However we could not show the correlation of the saturation changes and clinical outcome because of few numbers.

OIS imaging for multiple chemicals was recently reported [16,17,36,37]. In these studies, the scatter and the components of chromophores were important considerations

that were pointed out as areas that could be targeted to improve the accuracy of the

evaluation of hemodynamic changes. Therefore, further studies are required to examine

the metabolism of these different chemicals in the body and the specific wavelength(s)

of light that should be used for their OIS imaging. In the present study, we adopted the

HSC system to collect spectrally resolved data, and improved the analysis algorithm to

supplement the weak points of the light reflectance. In this study, we used the

components of the HbO, HbR, scatter, offset and residual. The inclusion of all

wavelengths avoided the removal of any data. We therefore consider that this approach

will more closely represent the data for the true neuronal metabolism. Using this

technique, we confirmed that the Hb-related wavelength data in human subjects were

similar to those obtained with SPECT, a spectroscopic technique commonly used in the

clinical setting. Generally, SPECT was performed in the chronic phase and can not be

performed intra-operatively, and the image resolution was not very high. However,

SPECT can express the whole brain hemodynamics, and this information can be used

for evaluating the patients' state. In contrast, the present technique could express the

partial cortical hemodynamics during an operation, and this information would be

useful for evaluating the cortical state. These two techniques would be able to

supplement each other, helping to obtain more accurate assessments of the

hemodynamic states of patients. However, the collection time using this procedure takes

several seconds. Therefore, future studies are required to improve the speed of this new

technique.

The potential of continuous spectral data analysis

Previous studies have performed an optical analysis of brain lesions and brain tissues [38-42], and the metabolism of lesions (e.g., brain tumors, epileptic foci, etc.) was found to be different from that of normal tissues [43,44]. Moreover, it was previously reported that the dynamic scattering properties were associated with the neuronal activity [45]. However, it is difficult to determine which components cause the differences in the light reflectance. As such, we typically use 5-aminolevulinic acid (5-ALA) fluorescence to detect brain tumors. The 5-ALA is converted to protoporphyrin IX (PpIX) in the body, and PpIX emits a red wavelength of light following excitation in the blue-violet spectrum [46]. Although this technique is commonly used during neurosurgery, PpIX is not specific for malignant tumors, since its formation depends on an abnormality in the porphyrin metabolism. Thus, to detect the lesion itself and to clearly define the edge of the lesion, more lesions-specific components and a more sensitive spectral analysis technique are needed. Some advanced studies have recently been reported that may lead to changes in this technique in the future [47,48].

In the present study, to confirm the utility of our HSC capture system and the analysis algorithm, we selected four components (HbO, HbR, scatter and offset) and one treated component (residual) for the spectral data analysis. The "residual" had different meaning from the other components, as the spectra of the other chemical substances were gathered in the residual; i.e., the residual could be separated into various spectra data. If we could thus determine new components associated with lesion-specific wavelengths, it would be possible to alter our program and convert the data into a suitable image for a lesion analysis. Therefore, this spectral analysis would be able to be reliable for not only future cortical hemodynamic studies, but also for

studying other neurological diseases, such as tumors, epileptic lesions and so on. Moreover, it might be possible to specify the intrinsic components related to the lesion to analyze the collected continuous spectral wavelength data included in the residual. Although it is necessary to improve the sensitivity and specificity of HSC for detecting the lesion-intrinsic signal, this technique may be useful for aiding therapeutic decisions during neurosurgery.

Conclusion

In this study, we adopted an HSC system that does not require a band-pass filter to collect the visible light wavelength data continuously, and improved the analysis algorithm to supplement the weak points of light reflectance techniques. We found that this continuous spectral data analysis method might therefore be a useful tool for evaluating the real-time cortical metabolism. Furthermore, with additional improvements to enable higher sensitivity and specificity, this technique may have the potential to aid in the therapeutic decision-making process during neurosurgery.

Conflict of interest

The authors declare no conflicts of interest in association with this study.

Reference

1. Mendelowitsch A, Sekhar LN, Clemente R, Shuaib A (1997) EC-IC bypass improves chronic ischemia in a patient with moyamoya disease secondary to sickle cell disease: an in vivo microdialysis study. Neurol Res 19 (1):66-70

2. Ishikawa T, Houkin K, Kamiyama H, Abe H (1997) Effects of surgical revascularization on outcome of patients with pediatric moyamoya disease. Stroke; a journal of cerebral circulation 28 (6):1170-1173

3. Rajamani K, Chaturvedi S (2007) Prevention of ischemic stroke: surgery. Current drug targets 8 (7):860-866

4. Hongo K, Kobayashi S, Okudera H, Hokama M, Nakagawa F (1995) Noninvasive Cerebral Optical Spectroscopy - Depth-Resolved Measurements of Cerebral Hemodynamics Using Indocyanine Green. Neurological research 17 (2):89-93

5. Towle EL, Richards LM, Shams Kazmi S, Fox DJ, Dunn AK (2012) Comparison of Indocyanine Green Angiography and Laser Speckle Contrast Imaging for the Assessment of Vasculature Perfusion. Neurosurgery 71 (5):1023-1030; discussion 1030-1021. doi:10.1227/NEU.0b013e31826adf88

6. Paul JS, Luft AR, Yew E, Sheu FS (2006) Imaging the development of an ischemic core following photochemically induced cortical infarction in rats using Laser Speckle Contrast Analysis (LASCA). Neuroimage 29 (1):38-45. doi:10.1016/j.neuroimage.2005.07.019

7. Dunn AK, Bolay H, Moskowitz MA, Boas DA (2001) Dynamic imaging of cerebral blood flow using laser speckle. Journal of cerebral blood flow and metabolism : official journal of the International Society of Cerebral Blood Flow and Metabolism 21 (3):195-201. doi:10.1097/00004647-200103000-00002

8. Sheth SA, Prakash N, Guiou M, Toga AW (2009) Validation and visualization of two-dimensional optical spectroscopic imaging of cerebral hemodynamics. Neuroimage 47 Suppl 2:T36-T43. doi:10.1016/j.neuroimage.2008.09.060

9. Prakash N, Uhlemann F, Sheth SA, Bookheimer S, Martin N, Toga AW (2009) Current trends in intraoperative optical imaging for functional brain mapping and delineation of lesions of language cortex. Neuroimage 47 Suppl 2:T116-126. doi:10.1016/j.neuroimage.2008.07.066

10. Casasent D, Chen XW (2004) Feature reduction and morphological processing for hyperspectral image data. Applied optics 43 (2):227-236

11. Bannon D (2009) Hyperspectral imaging: Cubes and slices. Nature Photonics 3 (11):627-629. doi:10.1038/nphoton.2009.205

12. Akbari H, Halig LV, Schuster DM, Osunkoya A, Master V, Nieh PT, Chen GZ, Fei B (2012) Hyperspectral imaging and quantitative analysis for prostate cancer detection. J Biomed Opt 17 (7):076005. doi:10.1117/1.JBO.17.7.076005

13. Goetz AF, Vane G, Solomon JE, Rock BN (1985) Imaging spectrometry for Earth remote sensing. Science 228 (4704):1147-1153. doi:10.1126/science.228.4704.1147

14. Jobsis FF, Keizer JH, LaManna JC, Rosenthal M (1977) Reflectance spectrophotometry of cytochrome aa3 in vivo. J Appl Physiol 43 (5):858-872

15. Sylvia AL, Rosenthal M (1979) Effects of age on brain oxidative metabolism in vivo. Brain research 165 (2):235-248

16. Wolf T, Lindauer U, Obrig H, Dreier J, Back T, Villringer A, Dirnagl U (1996) Systemic nitric oxide synthase inhibition does not affect brain oxygenation during cortical spreading depression in rats: a noninvasive near-infrared spectroscopy and laser-Doppler flowmetry study. Journal of cerebral blood flow and metabolism : official journal of the International Society of Cerebral Blood Flow and Metabolism 16 (6):1100-1107. doi:10.1097/00004647-199611000-00003

17. Yin C, Zhou F, Wang Y, Luo W, Luo Q, Li P (2013) Simultaneous detection of hemodynamics, mitochondrial metabolism and light scattering changes during cortical

spreading depression in rats based on multi-spectral optical imaging. Neuroimage 76:70-80. doi:10.1016/j.neuroimage.2013.02.079

18. Ellingsen PG, Nystrom S, Reitan NK, Lindgren M (2013) Spectral correlation analysis of amyloid beta plaque inhomogeneity from double staining experiments. J Biomed Opt 18 (10):101313. doi:10.1117/1.JBO.18.10.101313

19. Ellingsen PG, Reitan NK, Pedersen BD, Lindgren M (2013) Hyperspectral analysis using the correlation between image and reference. J Biomed Opt 18 (2):20501. doi:10.1117/1.JBO.18.2.020501

20. Satori S, Aoyanagi Y, Hara U, Mitsuhashi R, Takeuchi Y (2008) Hyperspectral sensor HSC3000 for nano-satellite 'TAIKI'. 7149:71490M-71490M-71499. doi:10.1117/12.804898

21. Zhang HF, Maslov K, Sivaramakrishnan M, Stoica G, Wang LV (2007) Imaging of hemoglobin oxygen saturation variations in single vessels in vivo using photoacoustic microscopy. Applied physics letters 90 (5):053901-053901-053903

22. Maslov K, Zhang HF, Wang LV (2007) Effects of wavelength-dependent fluence attenuation on the noninvasive photoacoustic imaging of hemoglobin oxygen saturation in subcutaneous vasculature in vivo. Inverse Problems 23 (6):S113

23. Frostig RD, Lieke EE, Ts'o DY, Grinvald A (1990) Cortical functional architecture and local coupling between neuronal activity and the microcirculation revealed by in vivo high-resolution optical imaging of intrinsic signals. Proceedings of the National Academy of Sciences 87 (16):6082-6086

24. Kashani AH, Kirkman E, Martin G, Humayun MS (2011) Hyperspectral computed tomographic imaging spectroscopy of vascular oxygen gradients in the rabbit retina in vivo. PloS one 6 (9):e24482

25. Subramanian NR, Kerekes JP, Kearney K, Schad N Spectral imaging of near-surface oxygen saturation. In: Medical Imaging, 2006. International Society for Optics and Photonics, pp 61423Y-61423Y-61429

26. Mirkovic J, Lau C, McGee S, Yu CC, Nazemi J, Galindo L, Feng V, Darragh T, de Las Morenas A, Crum C, Stier E, Feld M, Badizadegan K (2009) Effect of anatomy on spectroscopic detection of cervical dysplasia. J Biomed Opt 14 (4):044021. doi:10.1117/1.3194142

27. Ramella-Roman JC, Mathews SA, Kandimalla H, Nabili A, Duncan DD, D'Anna SA, Shah SM, Nguyen QD (2008) Measurement of oxygen saturation in the retina with a spectroscopic sensitive multi aperture camera. Opt Express 16 (9):6170-6182

28. Zhang RL, Chopp M, Zhang ZG, Jiang Q, Ewing JR (1997) A rat model of focal embolic cerebral ischemia. Brain research 766 (1-2):83-92

29. Kiyota Y, Pahlmark K, Memezawa H, Smith ML, Siesjo BK (1993) Free radicals and brain damage due to transient middle cerebral artery occlusion: the effect of dimethylthiourea. Experimental brain research Experimentelle Hirnforschung Experimentation cerebrale 95 (3):388-396

30. Li L, Ke Z, Tong KY, Ying M (2010) Evaluation of cerebral blood flow changes in focal cerebral ischemia rats by using transcranial Doppler ultrasonography. Ultrasound in medicine & biology 36 (4):595-603. doi:10.1016/j.ultrasmedbio.2010.01.005

31. Powers WJ, Press GA, Grubb RL, Jr., Gado M, Raichle ME (1987) The effect of hemodynamically significant carotid artery disease on the hemodynamic status of the cerebral circulation. Annals of internal medicine 106 (1):27-34

32. Baron JC, Bousser MG, Rey A, Guillard A, Comar D, Castaigne P (1981) Reversal of focal "misery-perfusion syndrome" by extra-intracranial arterial bypass in hemodynamic cerebral ischemia. A case study with 15O positron emission tomography. Stroke; a journal of cerebral circulation 12 (4):454-459

33. Awano T, Sakatani K, Yokose N, Kondo Y, Igarashi T, Hoshino T, Nakamura S, Fujiwara N, Murata Y, Katayama Y, Shikayama T, Miwa M (2010) Intraoperative EC-IC bypass blood

flow assessment with indocyanine green angiography in moyamoya and non-moyamoya ischemic stroke. World neurosurgery 73 (6):668-674. doi:10.1016/j.wneu.2010.03.027

34. Nakagawa A, Fujimura M, Arafune T, Sakuma I, Tominaga T (2009) Clinical implications of intraoperative infrared brain surface monitoring during superficial temporal artery-middle cerebral artery anastomosis in patients with moyamoya disease. J Neurosurg 111 (6):1158-1164. doi:10.3171/2009.4.JNS08585

35. Hoshino T, Katayama Y, Sakatani K, Kano T, Murata Y (2006) Intraoperative monitoring of cerebral blood oxygenation and hemodynamics during extracranial-intracranial bypass surgery by a newly developed visible light spectroscopy system. Surgical neurology 65 (6):569-576; discussion 576. doi:10.1016/j.surneu.2005.09.028

36. Sun X, Wang Y, Chen S, Luo W, Li P, Luo Q (2011) Simultaneous monitoring of intracellular pH changes and hemodynamic response during cortical spreading depression by fluorescence-corrected multimodal optical imaging. Neuroimage 57 (3):873-884. doi:10.1016/j.neuroimage.2011.05.040

37. Dunn AK, Devor A, Bolay H, Andermann ML, Moskowitz MA, Dale AM, Boas DA (2003) Simultaneous imaging of total cerebral hemoglobin concentration, oxygenation, and blood flow during functional activation. Opt Lett 28 (1):28-30

38. Eggert HR, Blazek V (1987) Optical properties of human brain tissue, meninges, and brain tumors in the spectral range of 200 to 900 nm. Neurosurgery 21 (4):459-464

39. Hochman DW (2000) Optical monitoring of neuronal activity: brain-mapping on a shoestring. Brain and cognition 42 (1):56-59. doi:10.1006/brcg.1999.1161

40. Haglund MM, Ojemann GA, Hochman DW (1992) Optical imaging of epileptiform and functional activity in human cerebral cortex. Nature 358 (6388):668-671. doi:10.1038/358668a0

41. Toms SA, Lin WC, Weil RJ, Johnson MD, Jansen ED, Mahadevan-Jansen A (2007) Intraoperative optical spectroscopy identifies infiltrating glioma margins with high sensitivity. Neurosurgery 61 (1 Suppl):327-335; discussion 335-326. doi:10.1227/01.neu.0000279226.68751.21

42. Lin WC, Sandberg DI, Bhatia S, Johnson M, Morrison G, Ragheb J (2009) Optical spectroscopy for in-vitro differentiation of pediatric neoplastic and epileptogenic brain lesions. J Biomed Opt 14 (1):014028. doi:10.1117/1.3080144

43. Kayama T, Yoshimoto T, Fujimoto S, Sakurai Y (1991) Intratumoral oxygen pressure in malignant brain tumor. J Neurosurg 74 (1):55-59. doi:10.3171/jns.1991.74.1.0055

44. Jensen RL (2009) Brain tumor hypoxia: tumorigenesis, angiogenesis, imaging, pseudoprogression, and as a therapeutic target. Journal of neuro-oncology 92 (3):317-335. doi:10.1007/s11060-009-9827-2

45. Graf BW, Ralston TS, Ko HJ, Boppart SA (2009) Detecting intrinsic scattering changes correlated to neuron action potentials using optical coherence imaging. Opt Express 17 (16):13447-13457

46. Stummer W, Stocker S, Wagner S, Stepp H, Fritsch C, Goetz C, Goetz AE, Kiefmann R, Reulen HJ (1998) Intraoperative detection of malignant gliomas by 5-aminolevulinic acid-induced porphyrin fluorescence. Neurosurgery 42 (3):518-525; discussion 525-516

47. Valdes PA, Leblond F, Jacobs VL, Wilson BC, Paulsen KD, Roberts DW (2012) Quantitative, spectrally-resolved intraoperative fluorescence imaging. Scientific reports 2:798. doi:10.1038/srep00798

48. Valdes PA, Kim A, Leblond F, Conde OM, Harris BT, Paulsen KD, Wilson BC, Roberts DW (2011) Combined fluorescence and reflectance spectroscopy for in vivo quantification of cancer biomarkers in low- and high-grade glioma surgery. J Biomed Opt 16 (11):116007. doi:10.1117/1.3646916

Figure Legends

Figure 1. HSC-1700 consists of a slit imaging spectrometer, the detector and an electrical assembly. The spectrometer is equipped with a direct vision prism and covers a wavelength range from 400-800 nm. The transmitting grating has a slit and relay lens unit. The transmitting grating has a slit and relay lens unit. The spectral specifications are customized by changing the scanning area.

Figure 2. The flow chart expressed the analysis procedure.

Figure 3. Calibration curves for the oxygen saturation of the "spectrometer" and the "HSC" were obtained using a spreadsheet for least squares. Each point was measured by the two instruments simultaneously. Twenty points of Hb spectra were measured and calculated, and a high correlation coefficient was observed for the curves.

Figure 4. The blood flow velocities (BFVs) were measured in the bilateral middle cerebral artery (MCA) during the MCA occlusion (MCAO) procedure using ultrasonography (US). The statistical significance of the differences in the BFV before and after the MCAO, and between the left and right BFV post-MCAO were evaluated by a two-sided t-test. $*P<0.03$, $**P<0.01$.

Figure 5. The middle cerebral artery occlusion (MCAO) model with the induction of cerebral infarcts in Wistar rats. The two slices of rat brains are different slices from one rat. Representative 2,3,4-triphenyltetrazolium chloride (TTC)-stained sections 12 hr after the MCAO procedure are shown.

Figure 6. Representative mapping images of the bilateral cerebral surfaces in response to the middle cerebral artery occlusion (MCAO) procedure. The areas other than the cortical surface are shown as a semitransparent gray color. HSC images could be converted to RGB images (A, D), relative Hb concentration (rHb-c) mapping images (B, E) and hemoglobin oxygen saturation mapping images (C, F). The RGB images of the animals after the MCAO procedure were similar to the pre-MCAO procedure images (A, D). In the rHb-c mapping images of the animals, the volume of hemoglobin in the bilateral hemisphere appeared to decrease after the MCAO procedure (B, E). However, in the hemoglobin oxygen saturation mapping images of the animals after the MCAO procedure, the saturation of the right hemisphere was lower than that of the left hemisphere (C, F).   Directions: P, posterior; R, right.

Figure 7. The location of the ROIs was the bilateral cortical surface of the MCA territory. The anatomical structures were used so that almost the same place (ROIs) could be pinpointed each time.

Figure 8. The values of saturation of the ROIs in the MCA territory were averaged, and the means were calculated. The statistical significance of the differences between the pre- and post-saturation values, and between the right and left saturation values, after MCAO were evaluated by a two-sided t-test. **$P<0.01$.

Figure 9. A representative case of moyamoya disease. These images were captured at the superficial temporal artery, the middle cerebral artery (STA-MCA) anastomosis (A,

B, C) and the post STA-MCA anastomosis (D, E, F). The areas other than the cortical surface are shown in a semitransparent gray color. The HSC spectral data were converted to RGB images (A, D), relative Hb concentration (rHb-c) mapping images (B, E) and saturation mapping images (C, F). The cerebral surface at the pre STA-MCA anastomosis (A). The cerebral surface at the post-STA-MCA anastomosis (D). The anastomosed STA is indicated by arrows (D). In the rHb-c mapping images of the post-STA-MCA anastomosis procedure, the Hb volume was slightly higher than that before the STA-MCA anastomosis (B, E). In the saturation mapping images of the post-STA-MCA anastomosis procedure, the cortical saturation was obviously higher than that of the data before the STA-MCA anastomosis (C, F). Directions: P, posterior; L, lateral.

Figure 10. The location of the ROIs was the cortical surface in the territory downstream of the STA-MCA anastomosis. The anatomical structures were used so that almost the same place (ROIs) could be pinpointed each time. Directions: P, posterior; L, lateral.

Figure 11. The cortical surface saturation values were averaged, and the mean was determined. The statistical significance of differences between the pre- and post-STA-MCA anastomosis saturation values were evaluated by a two-sided t-test. ***$P<0.001$.
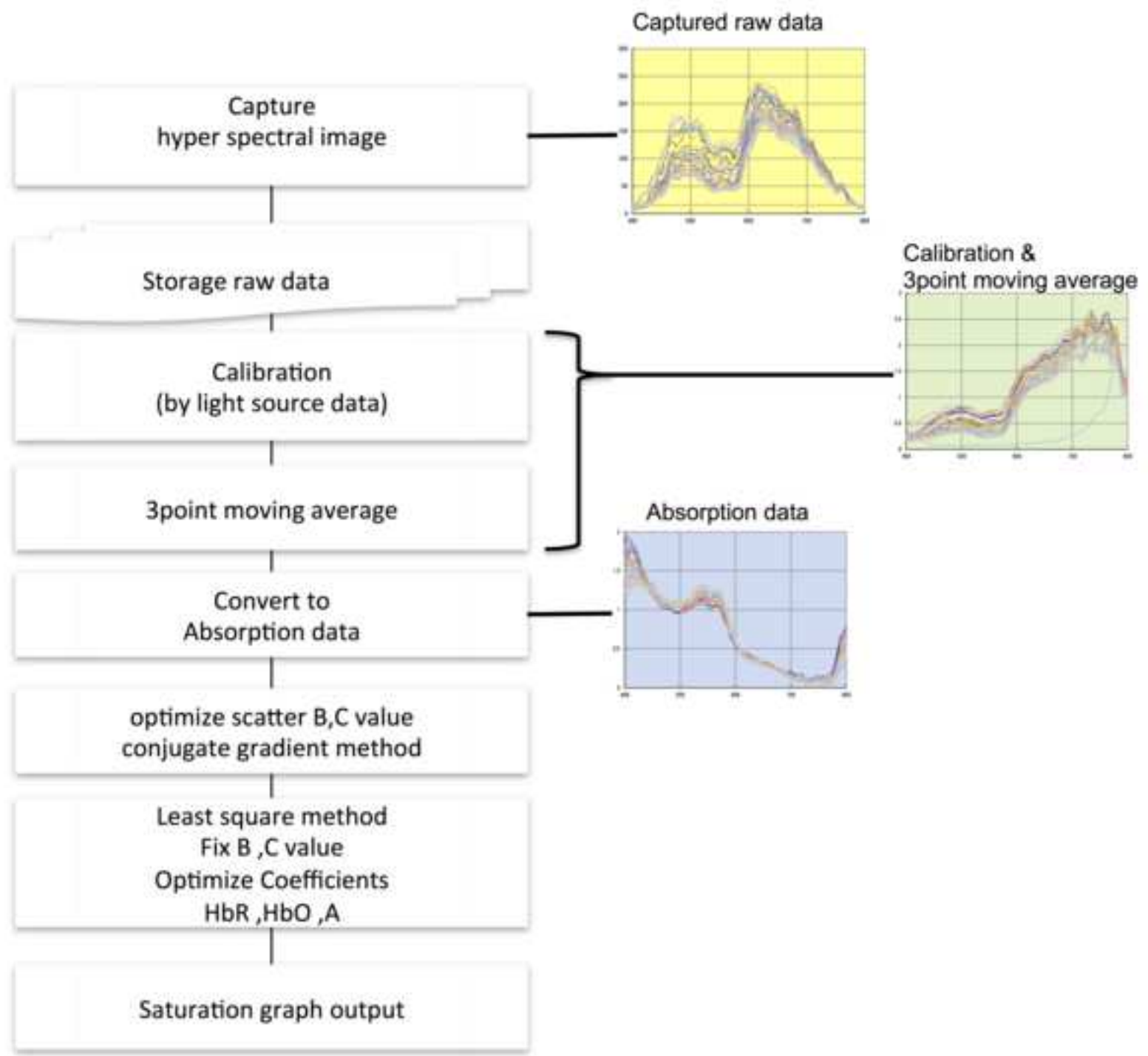
Figure

Captured raw data

Capture
hyper spectral image

Storage raw data

Calibration &
3point moving average

Calibration
(by light source data)

3point moving average

Absorption data

Convert to
Absorption data

optimize scatter B,C value
conjugate gradient method

Least square method
Fix B ,C value
Optimize Coefficients
HbR ,HbO ,A

Saturation graph output
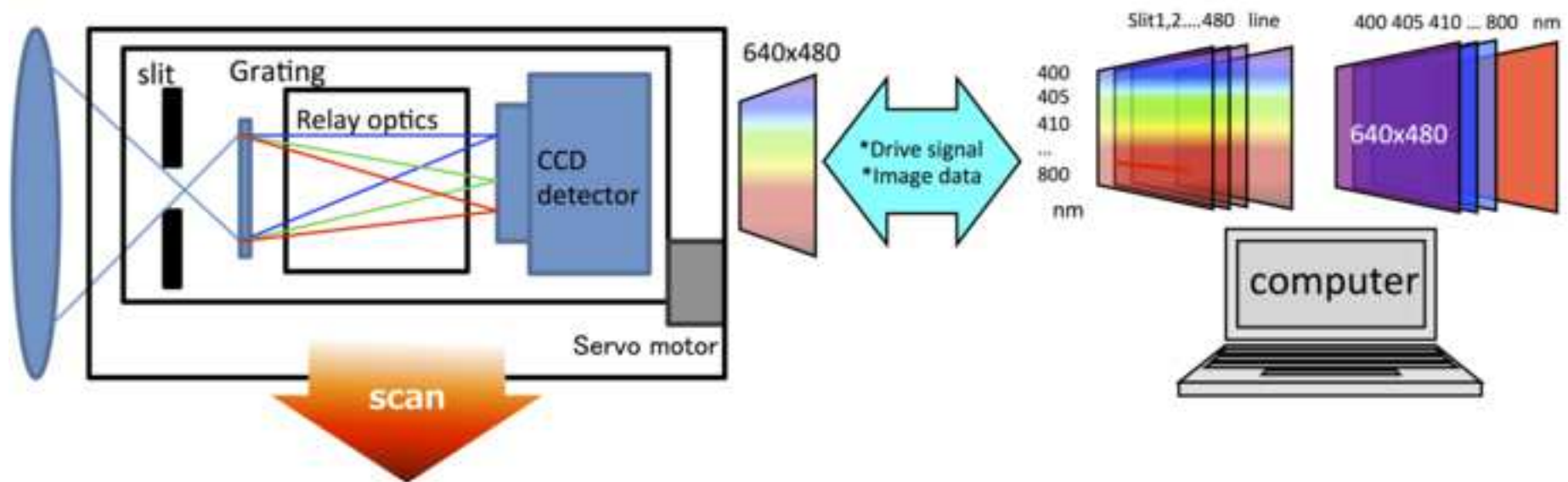
Calibration curve for spectrometer and Hyperspectral Camera

$y = 0.8547x + 0.0548$
$R^2 = 0.98195$

Oxygen saturation with Hyperspectral Camera (%)

Oxygen saturation with spectrometer (%)
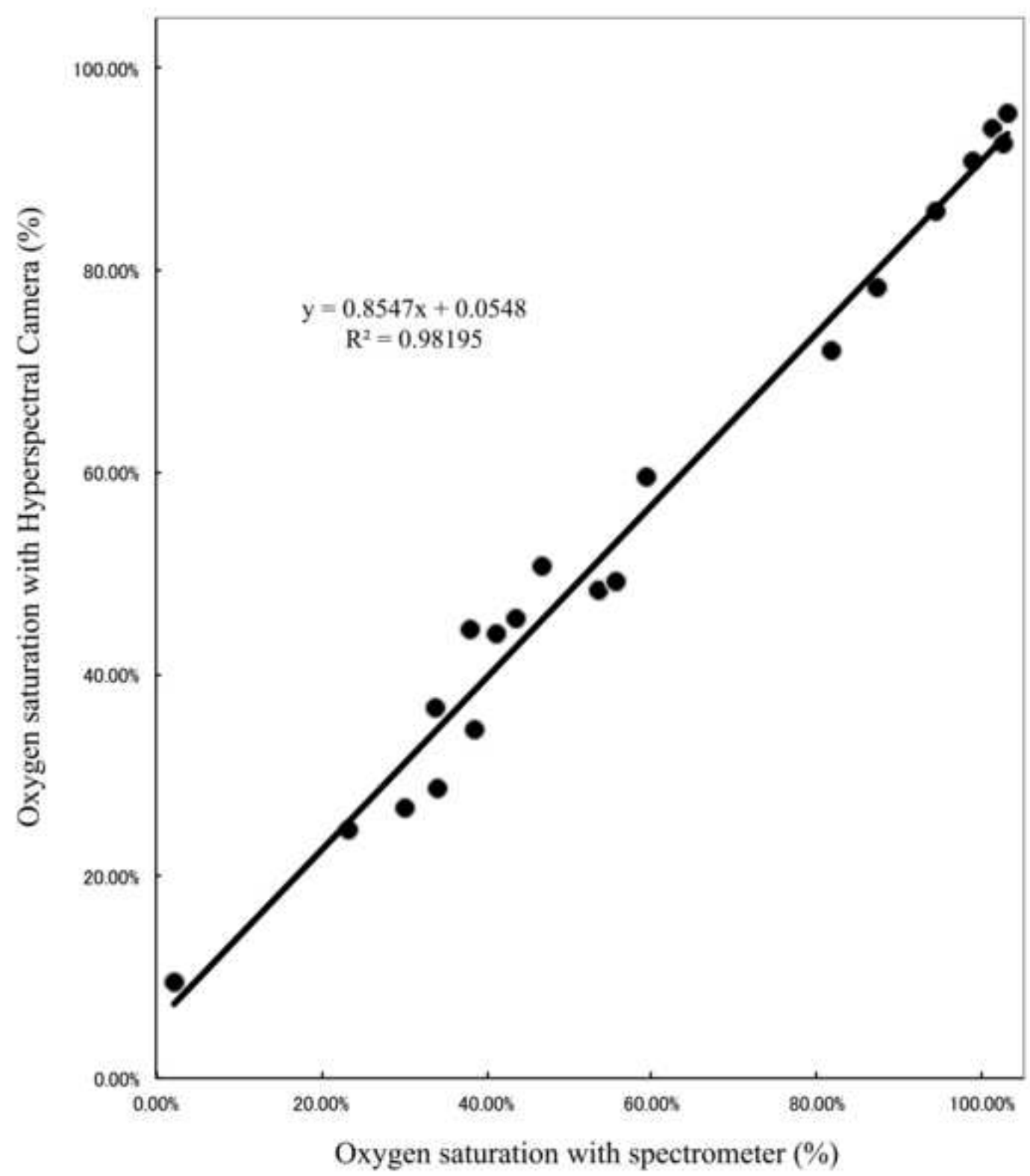
Blood flow changes of middle cerebral artery
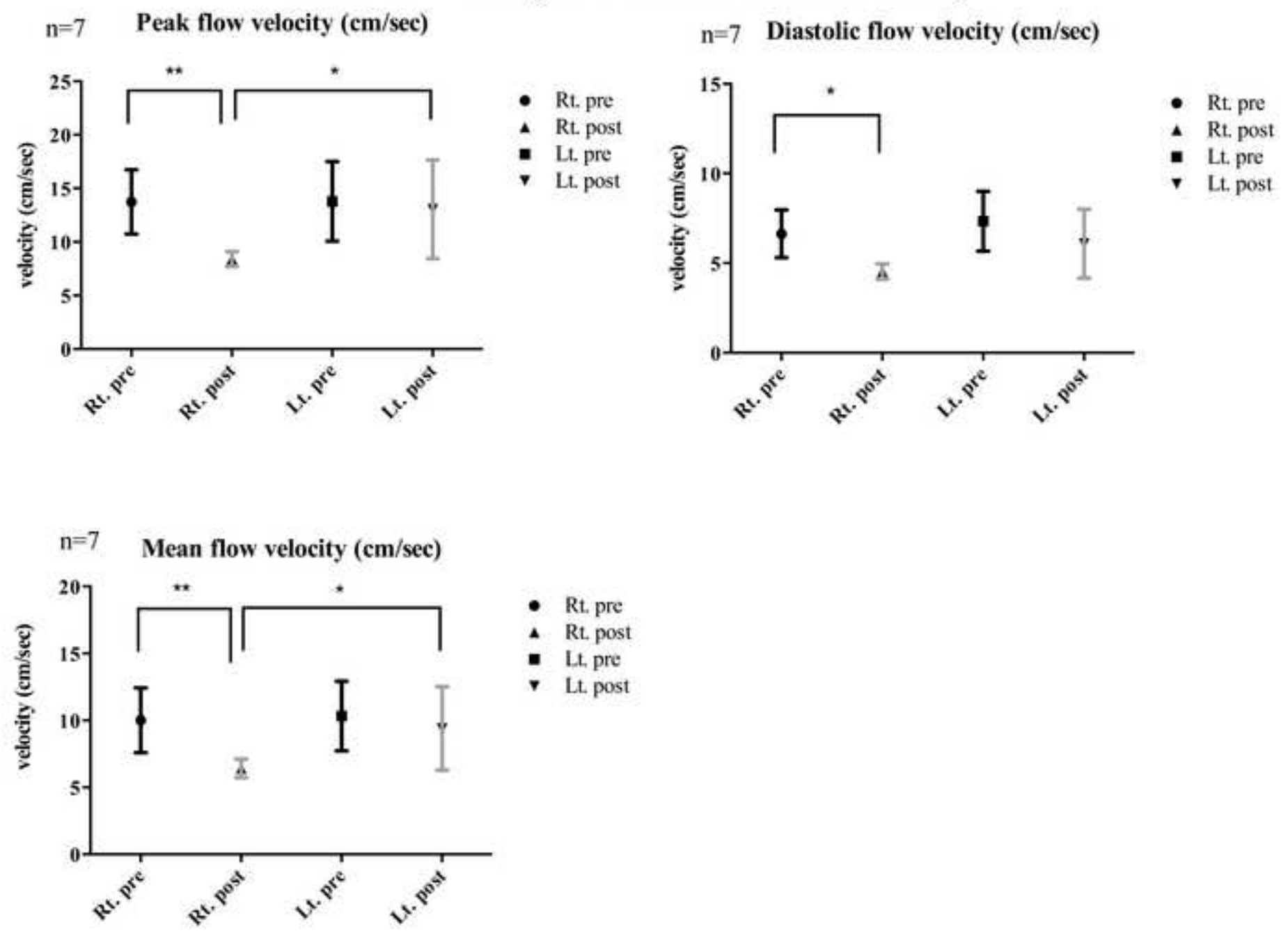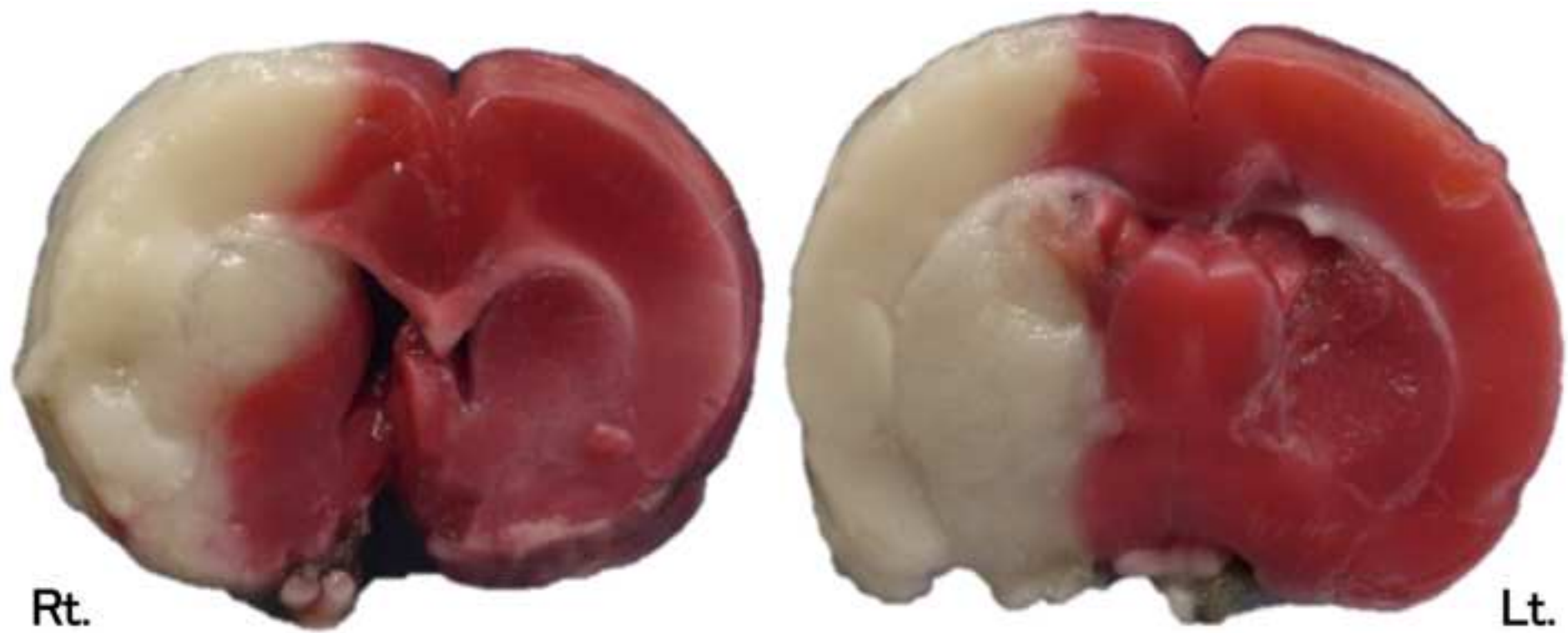
Rt.   Lt.
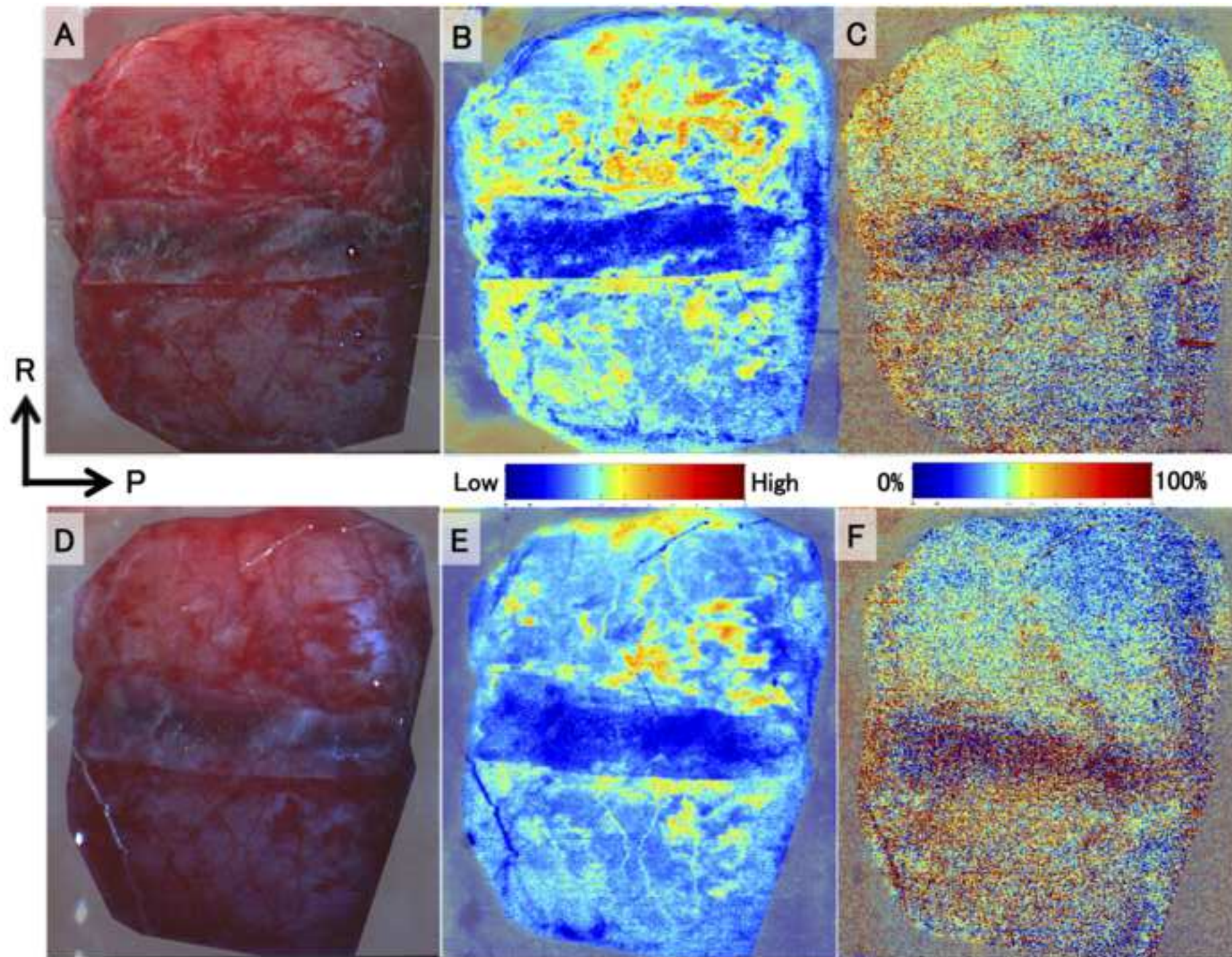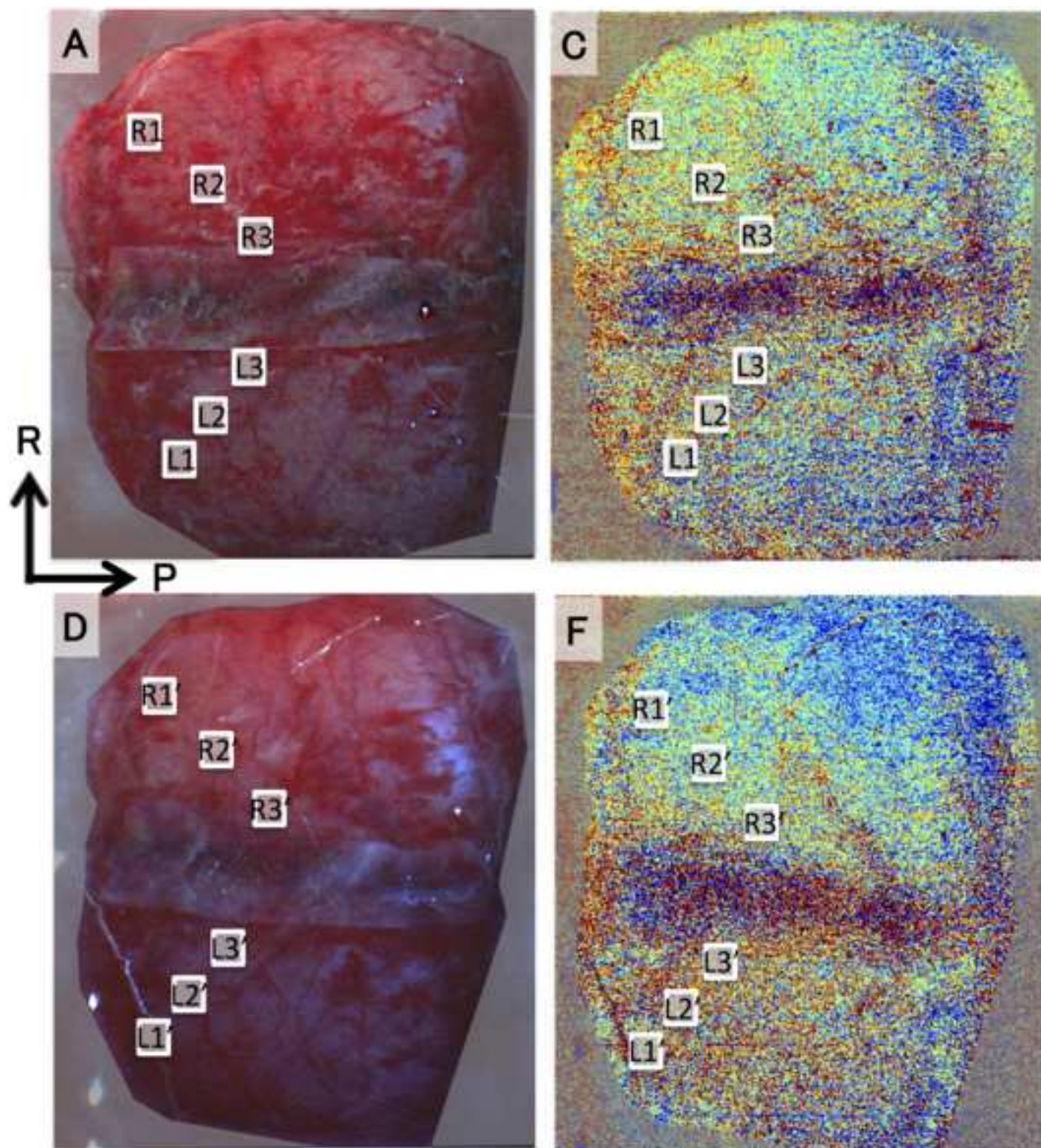
Oxygen saturation of rat cortical surface (%)
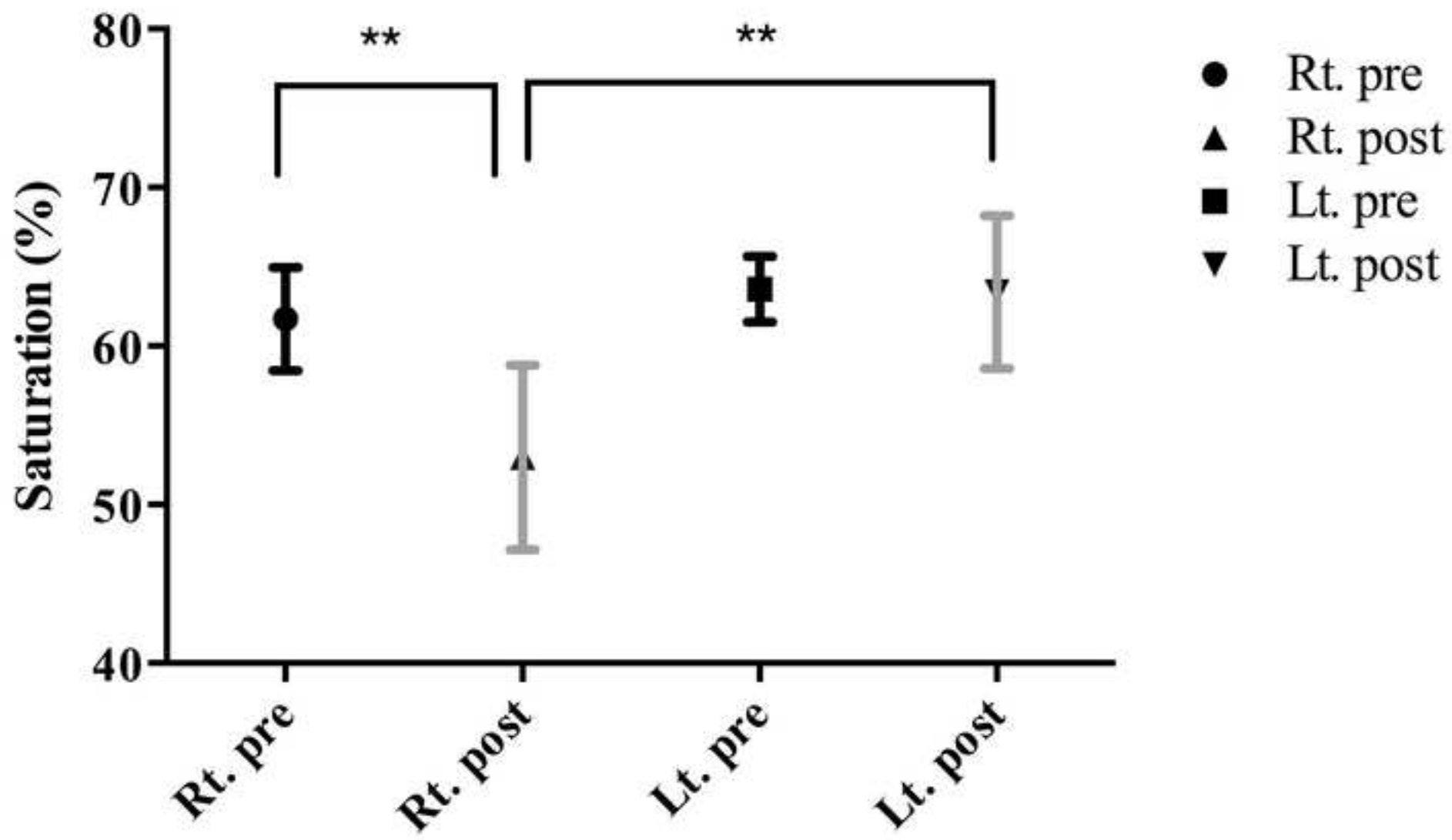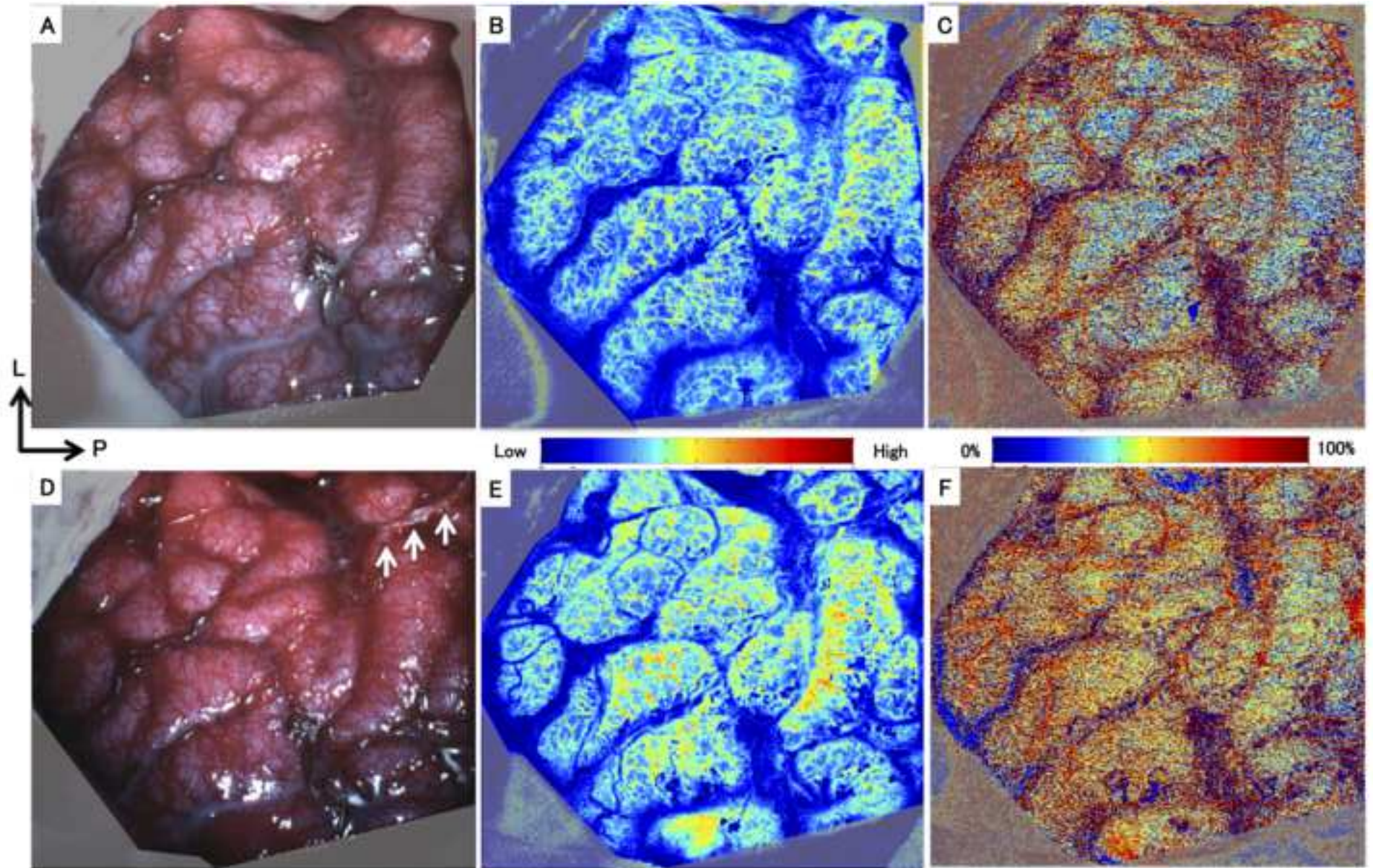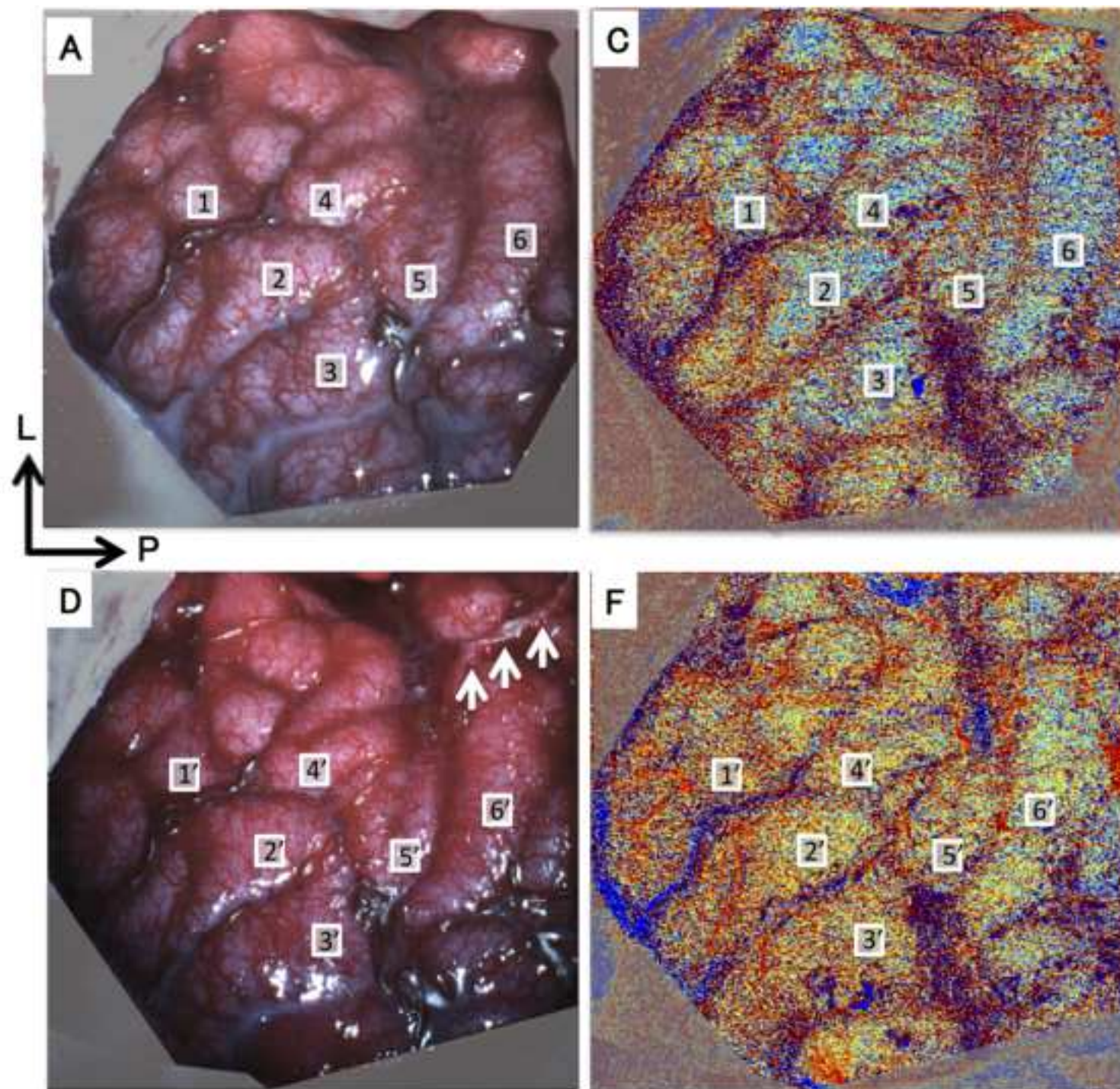
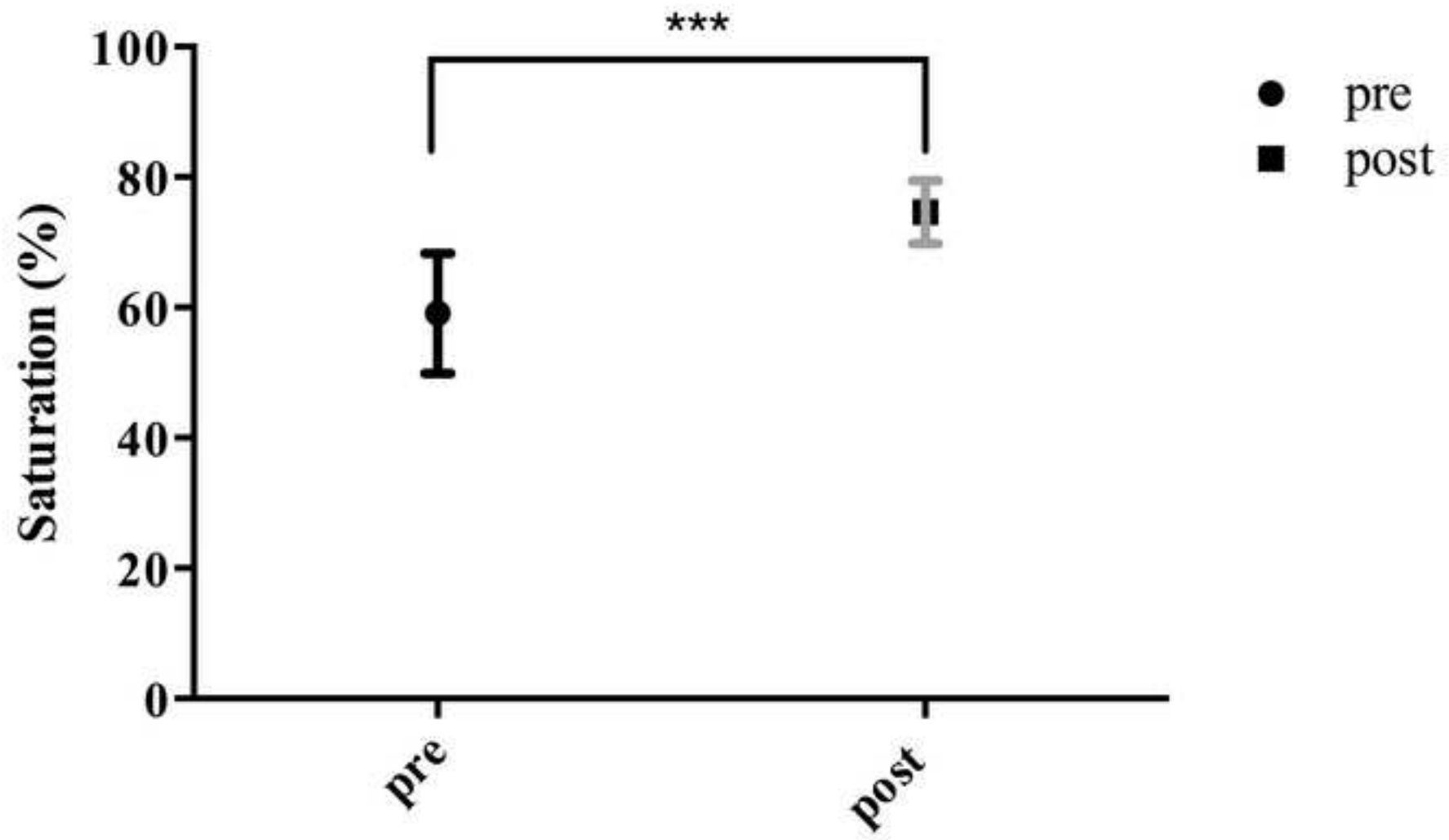Oxygen saturation of coritcal surface in clinical cases (%)

Table

Table 1

Individual Patients Profile and Intra-operative Physiological Parameters

Case no.	Age (y) / sex	Diagnosis	Anesthesia	pre/post STA-MCA anastomosis	RT (°C)	BT (°C)	ABP (mmHg)	HR (bpm)	FiO2	PaO2 (mmHg)	PaCO2 (mmHg)	EtCO2 (mmHg)
1	6/F	moyamoya disease	Air+O₂+N₂O+Sevoflurane+Fentanyl+Remifentanil	pre	26	36.9	100-134/40-60	100-120	0.4	269	38-40	44
				post	26	36.4	100-110/40-60	90-110	0.48	249	40.8	42
2	77/M	Rt. IC occlusion	Air+O₂+Propofol+Fentanyl+Remifentanil	pre	26.4	36.8	120-125/60-70	65-70	0.49	183	42.8	29
				post	26.6	36.5	140-160/70-90	70-75	0.49	227	36	45
3	66/M	Bil. IC occlusion	Air+O₂+Propofol+Fentanyl+Remifentanil	pre	25.8	35.4	120-130/40-60	45	0.46	232	39.1	35
				post	25.7	35.8	110-120/30-50	45	0.46	232	40.2	38
4	8/F	moyamoya disease	Air+O₂+N₂O+Sevoflurane+Fentanyl+Remifentanil	pre	26.5	36.7	120-130/40-60	90-95	0.46	192	42.2	39
				post	26.1	36.9	100-110/40-50	90-95	0.46	185	40.8	39

STA-MCA, surperficial temporal artery - middle cerebral artery; RT, room temperature; IC, Internal carotid artery; Bil., bilateral